

Deterministic Thermal Sculpting of Large-Scale 2D Semiconductor Nanocircuits

*Maria Caterina Giordano, Giorgio Zambito, Matteo Gardella,
and Francesco Buatier de Mongeot**

Dipartimento di Fisica, Università di Genova, Via Dodecaneso 33, 16146 - Genova, Italy

*E-mail: buatier@fisica.unige.it

Keywords: Large-area 2D TMD semiconductors, few-layer MoS₂ nanocircuits, thermal-Scanning Probe Lithography (t-SPL), *additive* nanolithography, Kelvin probe nanoscopy.

Abstract

Two-dimensional (2D) Transition Metal Dichalcogenide semiconductor (TMDs) nanocircuits are deterministically engineered over large-scale substrates. The original approach combines large-area physical growth of 2D TMDs layer with high resolution thermal - Scanning Probe Lithography (t-SPL), to re-shape the ultra-thin semiconducting layers at the nanoscale level. We demonstrate the *additive* nanofabrication of few-layer MoS₂ nanostructures, grown in the 2H-semiconducting TMD phase, as shown by their Raman vibrational fingerprints and by their optoelectronic response. The electronic signatures of the MoS₂ nanostructures are locally identified by Kelvin probe force microscopy providing chemical and compositional contrast at the nanometer scale. Finally, the potential role of the 2D TMD nanocircuits as building blocks of deterministic 2D semiconducting interconnections is demonstrated by high-resolution local conductivity maps showing the competitive transport properties of these large-area nanolayers. This work thus provides a powerful approach to scalable nanofabrication of 2D nano-interconnects and van der Waals heterostructures, and to their integration in real-world ultra-compact electronic and photonic nanodevices.

1. Introduction

Emerging two-dimensional (2D) materials belonging to the class of Transition Metal Dichalcogenide semiconductors (TMDs) have recently gained a broad interest by the scientific community offering new routes to nanoscience and nanotechnology.^{1–12} Thanks to their exceptional optoelectronic response and tunable bandgap in the Visible and Near-Infrared spectrum, combined with the atomically thin structure, functional properties can be obtained

with a strong impact in various fields ranging from nanoelectronics and nanophotonics, to energy conversion and quantum technologies.^{13–26} In this context the possibility to achieve a controlled reshaping of TMDs layers is particularly attracting in order to develop engineered and/or quantum confined 2D materials as a building block for functional nanodevices in electronics, photonics and quantum technologies^{6,27–33}. Recently the possibility to promote tuning of the optoelectronic response via shape engineering of 2D layers has been demonstrated using micrometric TMDs flakes^{34–36}, highlighting the impact of this approach in photonics and quantum optics. However few attempts can be found on the arbitrary nanolithography of 2D TMD layers on large-scale wafers, typically applied to isolated micro-flakes^{22,37,38}, or characterized by spatial resolution at the micro-scale.³⁹

So far, the most diffuse technique for 2D TMDs materials preparation has been mechanical exfoliation of crystals that provides randomly distributed 2D flakes, endowed with a size typically limited at the micro-scale. The urgent demand for potentially scalable platform and devices has recently motivated alternative growth methods for TMDs layers mainly relying on the Chemical Vapour Deposition (CVD) approach^{40–47} which leads to a random distribution of triangularly shaped 2D TMD islands typically sized on a micrometer scale. Complex multi-step lithography processes, requiring chemical or plasma etching of the 2D islands (subtractive approaches), are typically used for nanopatterning 2D TMDs, introducing unwanted contaminations or surface damages to the fragile ultra-thin layers.^{48,49} Scalable growth and non-invasive nanopatterning approaches are thus urgently required to engineer the optoelectronic and photonic response of 2D TMD layers.

The thermal-Scanning Probe Lithography (t-SPL) has recently emerged as a very promising technique, uniquely providing local modification of materials properties in ambient conditions with nanoscale spatial resolution provided by a sharp conductive probe^{50,51}. This approach is optimal for the fragile 2D layers as demonstrated by few recent experiments showing the nanolithography of high quality metallic contacts on 2D TMDs¹⁷, and their thermomechanical reshaping when exfoliated as micrometric flakes randomly distributed on the surface^{52,53}.

In this work we demonstrate a new *additive* approach enabling the scalable growth of ultra-thin 2D TMDs layer and their direct and high-resolution nano-sculpting via thermal-Scanning Probe Lithography. The nanolithography of ultra-thin MoS₂ nanocircuits deterministically located onto a large-scale wafer is demonstrated by combining the t-SPL of a sacrificial polymeric films, with large area ion beam assisted physical deposition of few-layer TMDs films. The Raman micro-spectroscopy maps have shown the characteristic vibrational response of the 2D

semiconductor nanopaths, spatially engineered thanks to the t-SPL based method. The non-invasive t-SPL has been further exploited to precisely align simple nanodevices based on high-quality metallic contacts onto the 2D TMDs nanopaths, uniquely preserving their electronic response. The capability to control the electronic transport properties at nanometer lateral scale is demonstrated via high-resolution Kelvin probe nanoscopy and local probing of the electric transport via conductive-AFM nanoscopy. The local electrical and compositional contrasts and the electrical conductivity, resolved at the nanometer scale on the MoS₂ nanopaths, qualify them as building blocks of next generation nanocircuitry. The exceptional uniformity of the 2D TMDs layers over large-area (cm²), combined with the non-invasive t-SPL nanolithography enables the precise nanofabrication of ultra-thin nanocircuits and van der Waals heterostructures nanodevices over large-scale wafers, opening new perspectives in electronics, photonics and quantum technologies.

2. Results and discussion

The homogeneous growth of ultra-thin MoS₂ layers over large-scale is demonstrated exploiting a new ion-beam assisted approach. Controlled deposition of ultra-thin semiconductor films is achieved via collimated ion beam sputtering (IBS) of a stoichiometric MoS₂ target, faced to the substrate (e.g. silica, silicon). Under this configuration large-area homogeneous films can be achieved on areas exceeding several cm², as highlighted by the sample picture of **Figure 1a**, which shows a few-layer MoS₂ film (thickness $\sim 6\text{nm}$) deposited on a transparent silica substrate. The deposition process of the pristine amorphous MoS₂ film takes place at room temperature and is thus compatible with flexible polymer substrates. Re-crystallization of MoS₂ films can be obtained via high temperature (750 °C) annealing in a tubular furnace, in presence of sulphur background pressure to avoid altering MoS₂ stoichiometry. The structural quality of the ultra-thin TMD film is confirmed by the Raman micro-spectra (**Figure 1b**) characterized by the E_{1g} and by the A_{1g} mode, resonant at 383 and 408 cm⁻¹ respectively, as expected for an ultra-thin MoS₂ layer⁵⁴. Remarkably the Raman response, detected over sub-micrometric optical spots, is homogeneous up to the cm scale, as demonstrated by the spectra acquired along a diagonal axis of the sample, 5-6 mm apart one from the other (red spots in Figure 1a). The presence of a 2H-semiconducting MoS₂ ultra-thin film is further confirmed by the optoelectronic response detected in far-field extinction spectroscopy (**Figure S1**), and characterized by the A and B exciton resonances⁵⁵.

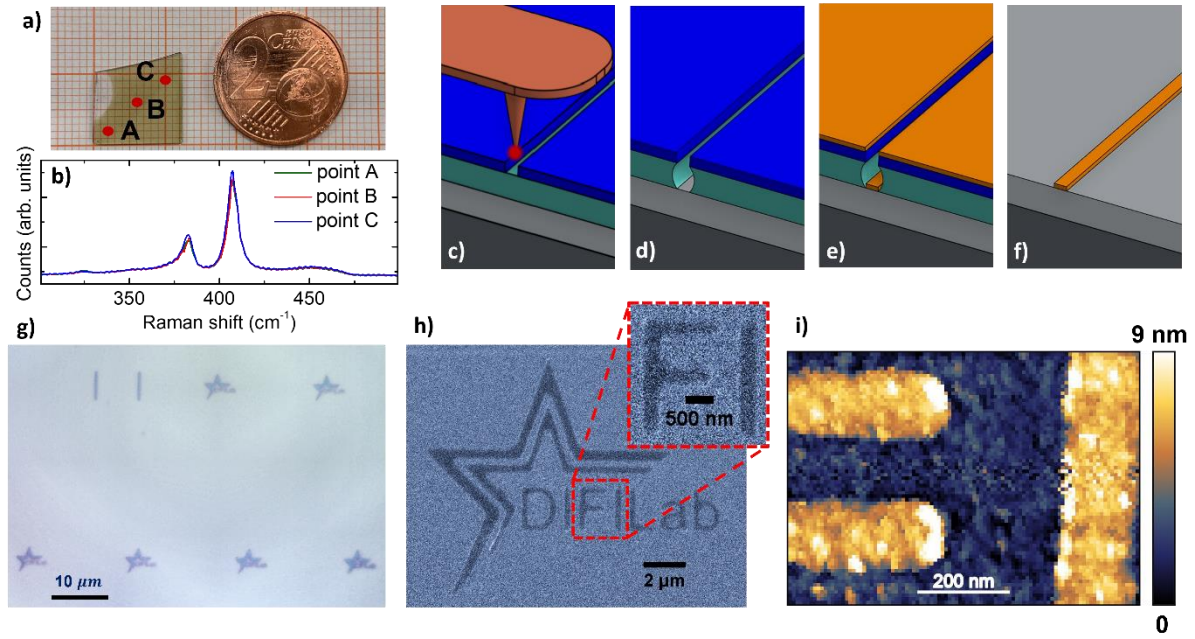


Figure 1. **a)** Picture of a large-scale ultra-thin MoS₂ layer grown onto a transparent silica substrate, and **b)** micro-Raman spectra detected in different spots of the samples shifted several mm apart one from the other (region A, B, C in the picture). **c-f)** Sketch of the t-SPL nanolithography process. **g)** Large-scale optical microscopy showing a series of MoS₂ nanocircuits fabricated onto a Si/SiO₂ substrate. **h)** SEM image of a few-layer MoS₂ nanocircuit (darker regions in the secondary electron signal) showing the logo of our laboratory (DIFILab facility - UNIGE) at the nanoscale, and zoom on a detail of the MoS₂ nanopaths. **i)** AFM image of a high resolution nanocircuit, showing ultra-thin MoS₂ nanopaths (scale bar 200 nm).

The large-scale homogeneity of these layers, combined with the novel t-SPL technique, provides the unique opportunity to develop a scalable approach for the nanoscale-resolved re-shaping of ultra-thin TMDs layers. The t-SPL indeed allows to pattern arbitrary nanopaths onto a thin polymeric bi-layer (see Methods) by exploiting a sharp hot nanoprobe (sketch in **Figure 1c**). In this way engineered nanopatterns can be *written* at high resolution (tip radius ~few nm) on the soft layer, which selectively exposes the substrate after due development process (**Figure 1d**). Hence the sacrificial bi-layer acts as a mask with appropriate negative angle profile for the following MoS₂ growth (**Figure 1e**). The final lift-off of the polymer film leaves behind engineered few-layer MoS₂ nanopaths, as sketched in **Figure 1f**.

The large-scale optical microscopy image of **Figure 1g** demonstrates the scalability of the method, enabling the *additive* nanofabrication of few-layer MoS₂ nanocircuits (darker regions of the image) in arbitrarily defined positions over large-scale, achieving uniform condition up

to the cm^2 scale. The zoomed Scanning Electron Microscopy (SEM) image on a specific nanopattern (**Figure 1h**) shows well defined MoS_2 nanopath (darker contrast in the SEM image) forming the logo of our facility and obtained thanks to the t-SPL nanolithography. The zoomed-in SEM image well highlights the contrast of the few-layer MoS_2 on the substrate with nm spatial resolution. Further MoS_2 nanopatterns designed at higher resolution with a thickness of 6.3 nm (~ 9 layers) are shown in the AFM image of **Figure 1i**, which evidences nanostripe widths below 200 nm. Remarkably, the *additive* nanolithography approach here described enables fabrication of clean ultra-thin MoS_2 nanostructures, avoiding damaging and/or contamination of the 2D TMDs layer intrinsic in the reactive ion etching based approach, typically used for nanopatterning 2D materials.^{48,56}

To confirm the material structure and to show the re-shaping capabilities of the few-layer material, Raman micro-spectra have been measured both on the engineered nanopaths (red curve in **Figure 2b** corresponding to blue regions of the optical microscopy image of **Figure 2a**) and few hundred nanometers apart on the bare substrate (black curve in Figure 2b). The Raman micro-spectrum detected on the MoS_2 nanopath shows the characteristic E_{2g}^1 and A_{1g} vibrational modes excited at 383 and 408 cm^{-1} , respectively, while on silica substrate (black curve) we measure an unstructured background.

In parallel, the high homogeneity of the few-layers MoS_2 nanopaths is demonstrated by the micro-Raman maps shown in **Figure 2c** and **Figure 2d** respectively, corresponding to the Raman image of a whole nano-logo and of a zoomed detail highlighted in Figure 2a. These Raman maps, obtained at an excitation wavelength of 532 nm, recover the morphology of the few-layer MoS_2 nanostructures, with a spatial resolution in the range of few hundred nm's which is only limited by optical diffraction (Figure 2d).

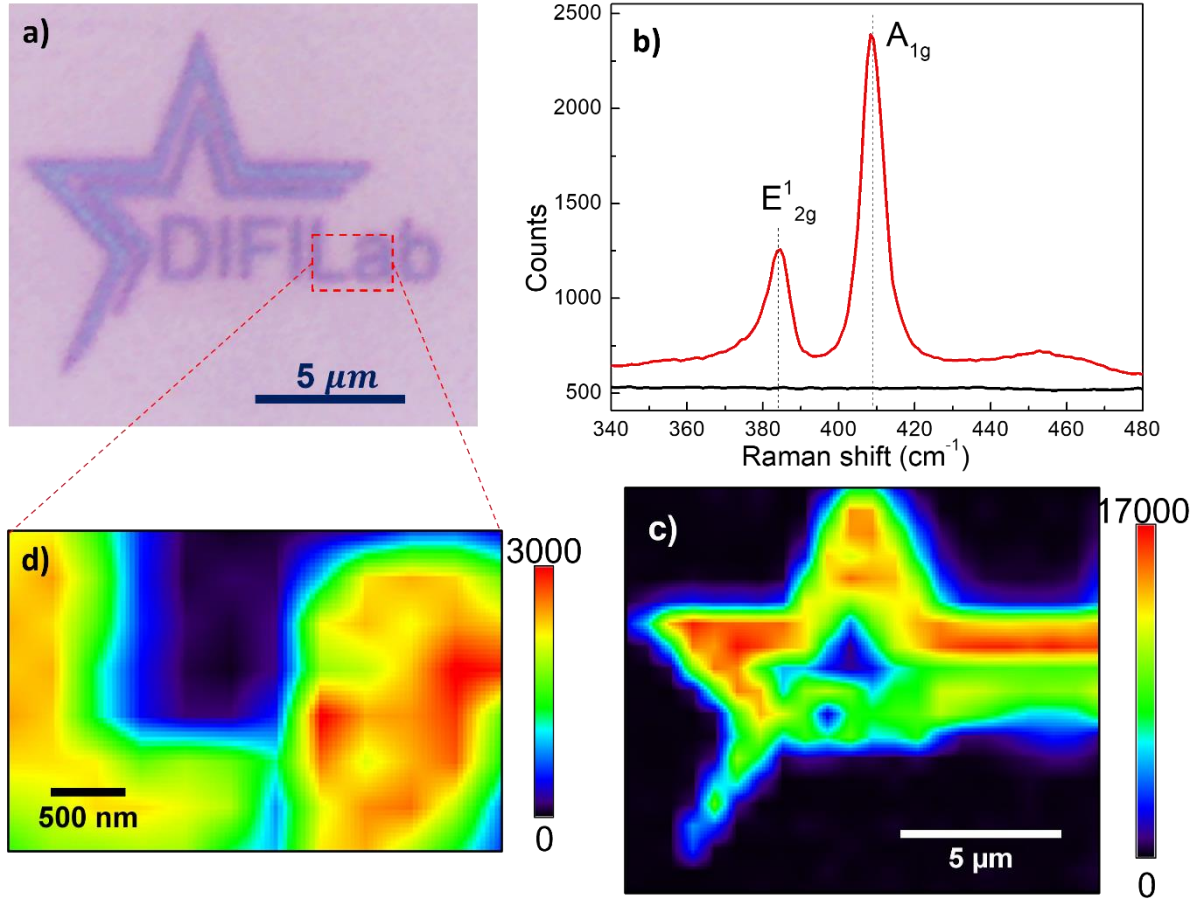


Figure 2. **a)** Optical microscopy image of a few-layer MoS₂ nanocircuit. **b)** Micro-Raman spectra detected on the MoS₂ nanopaths (red line) and on the neighboring Si region (black line). **c,d)** Micro-Raman maps detected on the whole MoS₂ nanocircuit and onto a detail (highlighted region in panel a), respectively. The maps show the signal detected in the range from 370 cm⁻¹ to 429 cm⁻¹, corresponding to E_{12g}¹ and A_{1g} modes.

In order to reveal the spatial arrangement of the MoS₂ nanostructure, overcoming the optical diffraction limit, and to investigate the local electrical properties Kelvin Probe Force Microscopy (KPFM) was employed. Such analysis was carried out by using a Pt-coated conductive tip operating in single pass configuration, in order to extract contact potential difference maps of MoS₂ nanopaths lying on a Si/SiO₂ substrate. We define the contact potential difference (CPD) referred to SiO₂ work function as:

$$\Delta_{CPD} = \frac{1}{e}(\phi_{SiO_2} - \phi_s)$$

where e is the elementary electron charge, ϕ_{SiO_2} is the silica work function and ϕ_s is the work function of the surface underneath the tip during the scan. **Figure 3a** shows the Δ_{CPD} map obtained on the MoS₂ nanopaths, highlighting their strong electrical contrast in terms of surface potential. An example of a Δ_{CPD} cross-section profile acquired across the MoS₂ nanotracks (white line in Figure 3a and corresponding profile in **Figure 3b**) shows a work function difference between MoS₂ nanopaths and silica substrate of about 200 meV. This electrical response is uniform over the CPD map, highlighting the MoS₂ to silica contrast with spatial resolution in the range of few tens of nm, determined by the Kelvin nanoprobe radius and by lock-in modulation voltage. In particular, the histogram of the Δ_{CPD} map (**Figure 3c**) is characterized by two distributions, respectively centered at 0 and -200 mV, as confirmed by the fit and by the cross-section profile at the MoS₂-silica edge. The former peak arises from the silica substrate and the latter from the MoS₂ nanopaths. The measured Δ_{CPD} map characterized by 200 mV contrast at the MoS₂-SiO₂ interface allows to quantify the work function of the MoS₂ nanopaths as $\phi_{MoS_2} \sim 5.25\text{eV}$, calculated considering the value of SiO₂ work function ($\sim 5.05\text{eV}$), in good agreement with respect to recent reports^{57,58}.

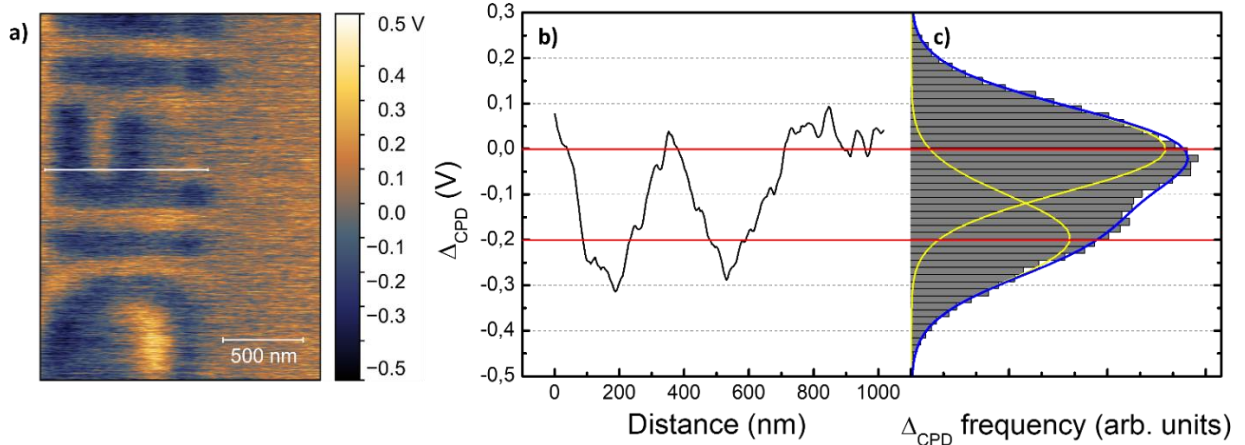


Figure 3: **a)** Kelvin Probe Microscopy image showing the Contact Potential Difference referred to silica work function ϕ_{SiO_2} (Δ_{CPD}) signal, characterized by a strong electrical contrast of the MoS₂ nanocircuits. **b,c)** Δ_{CPD} line profile corresponding to white line in panel a), and histogram of the detected CPD signal, respectively.

In order to show the potential of the 2D-TMDs nanocircuits as active optoelectronic interconnects, we devise a simple ultra-thin device thanks to the non-invasive t-SPL approach. High quality metallic contact can be precisely aligned onto the nanocircuits by exploiting the

peculiar in-situ imaging and real-time nanolithography capabilities (i.e. direct overlay method), avoiding undesired damage and contamination for the fragile layers¹⁷. In this way the electronic transport properties of the TMDs layers can be deeply investigated with nanoscale spatial resolution via conductive-AFM nanoscopy. **Figure 4** shows an example of 2D-TMDs device based onto a few-layer MoS₂ nanofinger. A metallic nanocontact (brighter finger at the bottom of the image) has been precisely aligned onto the few-layer nanofinger, thus enabling the local electric probing of the material with the conductive-AFM nanoprobe (ResiScope technology, sensitive across wide conductivity ranges). This c-AFM approach enabled the high-resolution detection of current and resistance maps onto the MoS₂ nanodevice, avoiding damage of the sample and/or the probe^{59,60}. The c-AFM maps were acquired in contact-AFM configuration by applying a DC bias voltage of 0.5 V to the sample (metallic nanoelectrode) with respect to a p-doped single crystal diamond tip.

Figure 4a and **Figure 4b** show the local-current and -resistance map of the MoS₂ nanofinger device, detected in real-time with the topography (**Figure 4c**). A strong electrical contrast is detected at the MoS₂-substrate edges within both the current and the resistance map, as highlighted in **Figure 4d** by a comparison between topography and local current extracted along a horizontal profile (white dashed line in **Figure 4a** and **Figure 4c**). The electrical maps demonstrate the semiconducting behavior of the MoS₂ nanocircuit device with nanoscale spatial resolution, precisely corresponding to the AFM topography. The resistance (current) map shows a lower resistance (higher current) in proximity of the nanoelectrode, while a gradual resistance increase (current decrease) is detected as the electronic mean path to the contact increases. To quantify this effect, a current profile, extracted along a vertical profile of **Figure 4a** (dashed red line), is shown in **Figure 4e**. Due to the strong anisotropy of the MoS₂ nanofinger, endowed with nanoscale width, this curve well represents our system. The experimental data (black dots) are well described by a power law function $I(d) \propto d^\alpha$ with $\alpha = -1.1$ (red line in **Figure 4e**), where d is the distance between the metal nanoelectrode and the conductive nanoprobe. This behavior well fits with the response of a semiconducting few-layer MoS₂ channel of length d whose resistance R_c is expected to scale as $R_c \propto \frac{1}{d}$. The local resistance maps allows to estimate a resistivity value of about 5 Ωm for these large-area few-layer MoS₂, under the approximation of a long channel device. This result is comparable to state of the art MoS₂ layers^{33,61,62} and very promising in view of deterministic 2D TMDs nano-interconnects. Furthermore, these few-layer nanofinger configuration highlights the possibility to engineer ever more complex few-layer van der Waals semiconducting nanodevices, taking

advantage of the non-invasive t-SPL nanolithography for the arbitrary and precise alignment of 2D materials endowed with their original optoelectronic properties.

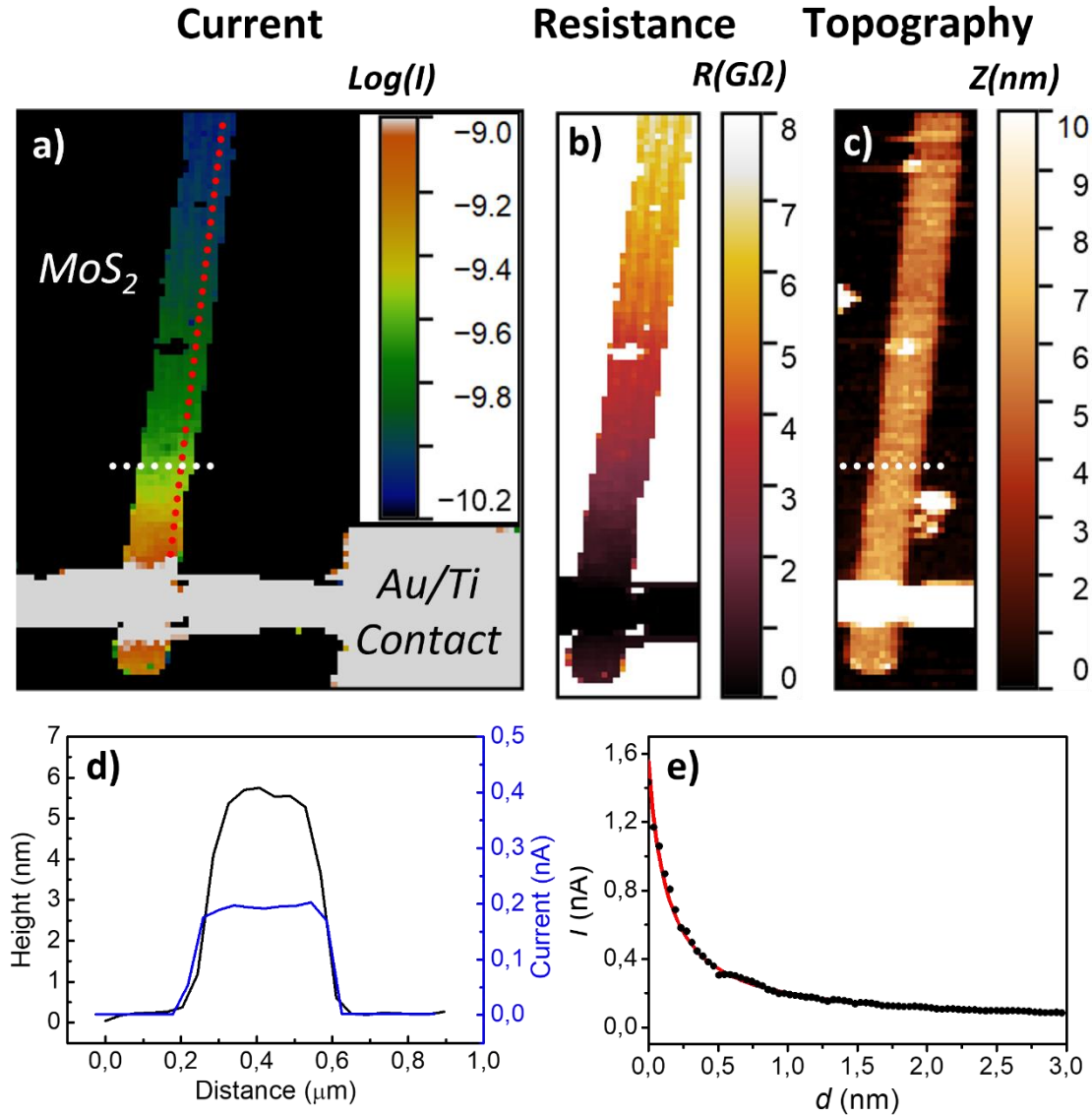


Figure 4 a-c) AFM current and corresponding local resistance and topography map of a few-layer MoS₂ nanostripe device under 0.5V DC bias. **d)** Current (blue) and corresponding topography (black) line profiles extracted across the substrate-finger edges (dashed white line in panel a and c). **e)** Current profile extracted from the current map of panel a) (dashed red line), showing a power law decay as the distance d from the nanocontact increases. A power law $I(d) \propto d^{-1.1}$ (red line) is superimposed to the data (black dots).

3. Conclusion

We have shown the *additive* nanolithography of few-layer MoS₂ nanocircuits arbitrarily and precisely engineered onto large-scale wafers, thanks to the non-invasive thermal-Scanning

Probe Lithography approach combined with the homogeneous growth of few-layer TMDs across several cm^2 . The thermal nanolithography of a sacrificial polymeric layer, combined with the large-scale physical deposition of the few-layer TMDs, uniquely enables the on-demand reshaping of ultra-thin TMDs layers with nanoscale spatial resolution. The so formed MoS_2 nanocircuits grow into the 2H-TMD semiconducting phase, as shown by their vibrational fingerprint in Raman micro-spectroscopy, and by their electrical work function in Kelvin probe nanoscopy. High quality few-layer TMDs nanodevices have been further engineered by exploiting the non-invasive t-SPL approach to precisely align metallic nanocontacts onto the MoS_2 nanocircuits. This configuration has enabled the local probing of the electronic transport properties of the few-layer MoS_2 nanocircuits, resolved via conductive-AFM nanoscopy. The local-conductivity maps highlight the competitive transport properties of these reshaped MoS_2 nanodevices as few-layer semiconducting interconnects in ultra-thin devices and components. Remarkably these results highlight the possibility to engineer even more complex van der Waals heterostructure nanodevices by this original t-SPL based technique, uniquely preserving the optoelectronic properties of the fragile few-layer materials. These reshaped 2D-TMDs nanocircuits thus open new perspectives for the integration of 2D semiconducting layers in scalable new-generation devices with impact in electronics, photonics, renewable energies and quantum technologies.

4. Methods

Large area growth of 2D TMDs

A fused silica (SiO_2) substrate is cleaned by ultrasound sonication both in acetone and isopropyl alcohol and loaded into a custom-made vacuum chamber with pressures of 10^{-6} / 10^{-7} mbar, faced towards a MoS_2 target. The latter is then irradiated by an ECR Plasma Source TPIS (TECTRA), which generates a 1.44 keV Ar^+ ion beam (gas purity N5.0) at a pressure of $6.0 \cdot 10^{-4}$ mbar. The ion beam forms a 45° angle with respect to the MoS_2 target surface normal. The ion beam irradiation induces the sputtering deposition of MoS_2 thin films on the SiO_2 substrate, while the thickness of the deposited material is monitored by means of a calibrated quartz crystal microbalance.

A single zone tubular furnace is used for the recrystallization process (sulphurization). The sample is placed at the center of the furnace, while a 10 sccm flux of inert gas (Ar) is fluxed inside the pipe as a carrier gas. A quartz boat with sulfur powder is placed between the origin

of the Ar flux and the sample. The furnace is then brought to the temperature of 750 °C with a heating ramp of 20°C/min and maintained at high temperature for a soaking time of 10 minutes. The heater is then turned off, allowing the cooldown of the sample.

thermal-Scanning Probe Lithography

The few layer MoS₂ nanocircuits are achieved thanks to the t-SPL patterning of a sacrificial bi-layer polymer mask, deposited by spin-coating onto a thermal oxide coated (SiO₂: 300 nm) p-doped silicon substrate. The underlying film is a PMMA/MA (thickness 95 nm) while a thermally sensitive film of polyphthalaldehyde (PPA - thickness 25 nm) is spin-coated on the surface. The new Nanofrazor Scholar setup (Heidelberg Instruments) enables the high-resolution t-SPL of the sensitive PPA film in ambient condition, thanks to the action of a sharp silicon tip (radius tip $\sim 10\text{nm}$) locally heating the surface. The system is able to provide temperature- and time-controlled heat pulses through the nanoprobe (temperature at the cantilever sensor tunable in the 500 °C - 1100 °C range), thus enabling the arbitrary nanolithography of complex shapes and/or local modification of material properties.

A chemical development of the PMMA/MA film underlying the patterned nanopaths is finally performed in order to expose the patterned areas of the substrate (solution of deionized water in isopropyl alcohol at 5% vol.).

The sample with the patterned bi-layer polymer mask is transferred in the UHV system for the physical large-scale MoS₂ growth, as for the extended flat films (see “Large area growth of 2D TMDs” section). The sample is finally rinsed in acetone for the lift-off of the non-patterned areas achieving MoS₂ nanopaths on the substrate, avoiding damages and contaminations by the lithographic process. Under this condition high quality MoS₂ nanostructures can be easily achieved with the high-temperature recrystallization process.

Metallic nanocontacts based on a Ti/Au thin film (thicknesses 2 nm/20 nm) are precisely aligned onto the MoS₂ nanocircuits (see as a sake of example the few-layer MoS₂ nanofinger device of Figure 4) thanks to in-situ imaging and direct t-SPL overlay nanopatterning based on the polymeric bilayer process.

Atomic Force Microscopy (AFM) characterization

High resolution AFM images have been acquired by a JPK NanoWizard AFM (Bruker) operating in Quantitative Imaging (QI) mode.

The Kelvin Probe Force Microscopy (KPFM) maps have been acquired by a Nano Observer AFM (Concept Scientific Instruments) operating in single-pass mode and equipped with a platinum-coated silicon tip. The conductive AFM maps (current, resistance) have been acquired by using the same Nano Observer AFM, equipped with a ResiScope module enabling c-AFM nanoscopy over wide current (and resistance) ranges avoiding damage to the sample. The c-AFM maps have been detected with a conductive p-doped diamond tip scanning in contact mode.

The analysis of all the AFM images has been performed with the software Gwyddion (open source).

Scanning Electron Microscopy (SEM) imaging

The top-view SEM topographies of the MoS₂ nanocircuits (secondary electron signal) have been acquired by exploiting a thermoionic electron source biased at 5 kV (Hitachi SEM SU3500).

Raman micro-spectroscopy

Raman micro-spectra and maps have been detected by using an NRS-4100 Raman microscope (JASCO) operating in back-scattering configuration with sample excitation with a 532 nm laser source.

Acknowledgements

All the authors acknowledge R. Chittofrati, E. Vigo, F. Bisio, C. Canale and P. Canepa for technical assistance and useful discussions.

F. Buatier de Mongeot and M. C. Giordano acknowledge financial support by Ministero dell'Università e della Ricerca, within the project 'Dipartimento di Eccellenza 2018-2022' art. 1, c. 314-337, Legge 232/2016.

F. Buatier de Mongeot acknowledges financial support by Università degli Studi di Genova within the project BIPE 2020.

M. C. Giordano acknowledges financial support by Ministero degli Affari Esteri e della Cooperazione Internazionale (MAECI) within 'Progetti di Grande Rilevanza 2021-2023' -

bilateral project Italy-Vietnam ‘Large-area 2D/plasmonic heterostructures for photocatalysis and energy storage (H2D)’.

G. Zambito acknowledges support from Compagnia di San Paolo for financing his PhD scholarship.

References

- (1) Huang, H. H.; Fan, X.; Singh, D. J.; Zheng, W. T. Recent Progress of TMD Nanomaterials: Phase Transitions and Applications. *Nanoscale* **2020**, *12* (3), 1247–1268. <https://doi.org/10.1039/C9NR08313H>.
- (2) Zhang, X.; Lai, Z.; Ma, Q.; Zhang, H. Novel Structured Transition Metal Dichalcogenide Nanosheets. *Chem. Soc. Rev.* **2018**, *47* (9), 3301–3338. <https://doi.org/10.1039/C8CS00094H>.
- (3) Li, S.; Lin, Y.-C.; Liu, X.-Y.; Hu, Z.; Wu, J.; Nakajima, H.; Liu, S.; Okazaki, T.; Chen, W.; Minari, T.; Sakuma, Y.; Tsukagoshi, K.; Suenaga, K.; Taniguchi, T.; Osada, M. Wafer-Scale and Deterministic Patterned Growth of Monolayer MoS₂ via Vapor–Liquid–Solid Method. *Nanoscale* **2019**, *11* (34), 16122–16129. <https://doi.org/10.1039/C9NR04612G>.
- (4) He, F.; Zhou, Y.; Ye, Z.; Cho, S.-H.; Jeong, J.; Meng, X.; Wang, Y. Moiré Patterns in 2D Materials: A Review. *ACS Nano* **2021**, *15* (4), 5944–5958. <https://doi.org/10.1021/acsnano.0c10435>.
- (5) Trovatello, C.; Miranda, H. P. C.; Molina-Sánchez, A.; Borrego-Varillas, R.; Manzoni, C.; Moretti, L.; Ganzer, L.; Maiuri, M.; Wang, J.; Dumcenco, D.; Kis, A.; Wirtz, L.; Marini, A.; Soavi, G.; Ferrari, A. C.; Cerullo, G.; Sangalli, D.; Conte, S. D. Strongly Coupled Coherent Phonons in Single-Layer MoS₂. *ACS Nano* **2020**, *14* (5), 5700–5710. <https://doi.org/10.1021/acsnano.0c00309>.
- (6) van de Groep, J.; Song, J.-H.; Celano, U.; Li, Q.; Kik, P. G.; Brongersma, M. L. Exciton Resonance Tuning of an Atomically Thin Lens. *Nat. Photonics* **2020**, *14* (7), 426–430. <https://doi.org/10.1038/s41566-020-0624-y>.
- (7) Chen, J.; Zhu, J.; Wang, Q.; Wan, J.; Liu, R. Homogeneous 2D MoTe₂ CMOS Inverters and p–n Junctions Formed by Laser-Irradiation-Induced P-Type Doping. *Small* **2020**, *16* (30), 2001428. <https://doi.org/10.1002/sml.202001428>.
- (8) Verre, R.; Baranov, D. G.; Munkhbat, B.; Cuadra, J.; Käll, M.; Shegai, T. Transition Metal Dichalcogenide Nanodisks as High-Index Dielectric Mie Nanoresonators. *Nature Nanotechnology* **2019**, *14* (7), 679–683. <https://doi.org/10.1038/s41565-019-0442-x>.
- (9) Voiry, D.; Yang, J.; Chhowalla, M. Recent Strategies for Improving the Catalytic Activity of 2D TMD Nanosheets Toward the Hydrogen Evolution Reaction. *Advanced Materials* **2016**, *28* (29), 6197–6206. <https://doi.org/10.1002/adma.201505597>.
- (10) Deng, M.; Li, Z.; Rong, X.; Luo, Y.; Li, B.; Zheng, L.; Wang, X.; Lin, F.; Meixner, A. J.; Braun, K.; Zhu, X.; Fang, Z. Light-Controlled Near-Field Energy Transfer in Plasmonic Metasurface Coupled MoS₂ Monolayer. *Small* **2020**, *16* (40), 2003539. <https://doi.org/10.1002/sml.202003539>.
- (11) Bao, X.; Ou, Q.; Xu, Z.-Q.; Zhang, Y.; Bao, Q.; Zhang, H. Band Structure Engineering in 2D Materials for Optoelectronic Applications. *Advanced Materials Technologies* **2018**, *3* (11), 1800072. <https://doi.org/10.1002/admt.201800072>.
- (12) Wang, Q. H.; Kalantar-Zadeh, K.; Kis, A.; Coleman, J. N.; Strano, M. S. Electronics and Optoelectronics of Two-Dimensional Transition Metal Dichalcogenides. *Nature Nanotechnology* **2012**, *7* (11), 699–712. <https://doi.org/10.1038/nnano.2012.193>.

- (13) Sriram, P.; Manikandan, A.; Chuang, F.; Chueh, Y. Hybridizing Plasmonic Materials with 2D-Transition Metal Dichalcogenides toward Functional Applications. *Small* **2020**, *16* (15), 1904271. <https://doi.org/10.1002/sml.201904271>.
- (14) Sun, J.; Li, Y.; Hu, H.; Chen, W.; Zheng, D.; Zhang, S.; Xu, H. Strong Plasmon–Exciton Coupling in Transition Metal Dichalcogenides and Plasmonic Nanostructures. *Nanoscale* **2021**, *13* (8), 4408–4419. <https://doi.org/10.1039/D0NR08592H>.
- (15) Genco, A.; Cerullo, G. Optical Nonlinearity Goes Ultrafast in 2D Semiconductor-Based Nanocavities. *Light Sci Appl* **2022**, *11* (1), 127. <https://doi.org/10.1038/s41377-022-00827-3>.
- (16) Maeso, D.; Castellanos-Gomez, A.; Agraït, N.; Rubio-Bollinger, G. Fast Yet Quantum-Efficient Few-Layer Vertical MoS₂ Photodetectors. *Advanced Electronic Materials* **2019**, *5* (7), 1900141. <https://doi.org/10.1002/aelm.201900141>.
- (17) Zheng, X.; Calò, A.; Albisetti, E.; Liu, X.; Alharbi, A. S. M.; Arefe, G.; Liu, X.; Spieser, M.; Yoo, W. J.; Taniguchi, T.; Watanabe, K.; Aruta, C.; Ciarrocchi, A.; Kis, A.; Lee, B. S.; Lipson, M.; Hone, J.; Shahrjerdi, D.; Riedo, E. Patterning Metal Contacts on Monolayer MoS₂ with Vanishing Schottky Barriers Using Thermal Nanolithography. *Nat Electron* **2019**, *2* (1), 17–25. <https://doi.org/10.1038/s41928-018-0191-0>.
- (18) Zhang, H.; Abhiraman, B.; Zhang, Q.; Miao, J.; Jo, K.; Roccasacca, S.; Knight, M. W.; Davoyan, A. R.; Jariwala, D. Hybrid Exciton-Plasmon-Polaritons in van Der Waals Semiconductor Gratings. *Nature Communications* **2020**, *11* (1). <https://doi.org/10.1038/s41467-020-17313-2>.
- (19) Bucher, T.; Vaskin, A.; Mupparapu, R.; Löchner, F. J. F.; George, A.; Chong, K. E.; Fasold, S.; Neumann, C.; Choi, D.-Y.; Eilenberger, F.; Setzpfandt, F.; Kivshar, Y. S.; Pertsch, T.; Turchanin, A.; Staude, I. Tailoring Photoluminescence from MoS₂ Monolayers by Mie-Resonant Metasurfaces. *ACS Photonics* **2019**, *6* (4), 1002–1009. <https://doi.org/10.1021/acsphotonics.8b01771>.
- (20) Bhatnagar, M.; Giordano, M. C.; Mennucci, C.; Chowdhury, D.; Mazzanti, A.; Della Valle, G.; Martella, C.; Tummala, P.; Lamperti, A.; Molle, A.; Buatier de Mongeot, F. Ultra-Broadband Photon Harvesting in Large-Area Few-Layer MoS₂ Nanostripe Gratings. *Nanoscale* **2020**, *12* (48), 24385–24393. <https://doi.org/10.1039/D0NR06744J>.
- (21) Wong, J.; Jariwala, D.; Tagliabue, G.; Tat, K.; Davoyan, A. R.; Sherrott, M. C.; Atwater, H. A. High Photovoltaic Quantum Efficiency in Ultrathin van Der Waals Heterostructures. *ACS Nano* **2017**, *11* (7), 7230–7240. <https://doi.org/10.1021/acs.nano.7b03148>.
- (22) Palacios-Berraquero, C.; Kara, D. M.; Montblanch, A. R.-P.; Barbone, M.; Latawiec, P.; Yoon, D.; Ott, A. K.; Loncar, M.; Ferrari, A. C.; Atatüre, M. Large-Scale Quantum-Emitter Arrays in Atomically Thin Semiconductors. *Nature Communications* **2017**, *8* (1). <https://doi.org/10.1038/ncomms15093>.
- (23) Martella, C.; Mennucci, C.; Lamperti, A.; Cappelluti, E.; de Mongeot, F. B.; Molle, A. Designer Shape Anisotropy on Transition-Metal-Dichalcogenide Nanosheets. *Advanced Materials* **2018**, *30* (9), 1705615. <https://doi.org/10.1002/adma.201705615>.
- (24) Schaibley, J. R.; Yu, H.; Clark, G.; Rivera, P.; Ross, J. S.; Seyler, K. L.; Yao, W.; Xu, X. Valleytronics in 2D Materials. *Nature Reviews Materials* **2016**, *1* (11). <https://doi.org/10.1038/natrevmats.2016.55>.
- (25) Wang, K.; Wang, J.; Fan, J.; Lotya, M.; O'Neill, A.; Fox, D.; Feng, Y.; Zhang, X.; Jiang, B.; Zhao, Q.; Zhang, H.; Coleman, J. N.; Zhang, L.; Blau, W. J. Ultrafast Saturable Absorption of Two-Dimensional MoS₂ Nanosheets. *ACS Nano* **2013**, *7* (10), 9260–9267. <https://doi.org/10.1021/nn403886t>.

- (26) Giannazzo, F.; Greco, G.; Roccaforte, F.; Mahata, C.; Lanza, M. Conductive AFM of 2D Materials and Heterostructures for Nanoelectronics. In *Electrical Atomic Force Microscopy for Nanoelectronics*; Celano, U., Ed.; NanoScience and Technology; Springer International Publishing: Cham, 2019; pp 303–350. https://doi.org/10.1007/978-3-030-15612-1_10.
- (27) Stanford, M. G.; Rack, P. D.; Jariwala, D. Emerging Nanofabrication and Quantum Confinement Techniques for 2D Materials beyond Graphene. *npj 2D Materials and Applications* **2018**, 2 (1). <https://doi.org/10.1038/s41699-018-0065-3>.
- (28) Spreyer, F.; Ruppert, C.; Georgi, P.; Zentgraf, T. Influence of Plasmon Resonances and Symmetry Effects on Second Harmonic Generation in WS₂–Plasmonic Hybrid Metasurfaces. *ACS Nano* **2021**, 15 (10), 16719–16728. <https://doi.org/10.1021/acsnano.1c06693>.
- (29) Bhatnagar, M.; Gardella, M.; Giordano, M. C.; Chowdhury, D.; Mennucci, C.; Mazzanti, A.; Valle, G. D.; Martella, C.; Tummala, P.; Lamperti, A.; Molle, A.; Buatier de Mongeot, F. Broadband and Tunable Light Harvesting in Nanorippled MoS₂ Ultrathin Films. *ACS Appl. Mater. Interfaces* **2021**, 13 (11), 13508–13516. <https://doi.org/10.1021/acsaami.0c20387>.
- (30) Giordano, M. C.; Viti, L.; Mitrofanov, O.; Vitiello, M. S. Phase-Sensitive Terahertz Imaging Using Room-Temperature near-Field Nanodetectors. *Optica* **2018**, 5 (5), 651. <https://doi.org/10.1364/OPTICA.5.000651>.
- (31) Telesio, F.; le Gal, G.; Serrano-Ruiz, M.; Prescimone, F.; Toffanin, S.; Peruzzini, M.; Heun, S. Ohmic Contact Engineering in Few-Layer Black Phosphorus: Approaching the Quantum Limit. *Nanotechnology* **2020**, 31 (33), 334002. <https://doi.org/10.1088/1361-6528/ab8cf4>.
- (32) Ly, T. H.; Zhao, J.; Kim, H.; Han, G. H.; Nam, H.; Lee, Y. H. Vertically Conductive MoS₂ Spiral Pyramid. *Adv. Mater.* **2016**, 28 (35), 7723–7728. <https://doi.org/10.1002/adma.201602328>.
- (33) Wang, B.; Yang, S.; Wang, C.; Wu, M.; Huang, L.; Liu, Q.; Jiang, C. Enhanced Current Rectification and Self-Powered Photoresponse in Multilayer p-MoTe₂/n-MoS₂ van Der Waals Heterojunctions. *Nanoscale* **2017**, 9 (30), 10733–10740. <https://doi.org/10.1039/C7NR03445H>.
- (34) Castellanos-Gomez, A.; Roldán, R.; Cappelluti, E.; Buscema, M.; Guinea, F.; van der Zant, H. S. J.; Steele, G. A. Local Strain Engineering in Atomically Thin MoS₂. *Nano Letters* **2013**, 13 (11), 5361–5366. <https://doi.org/10.1021/nl402875m>.
- (35) Yang, J.; Wang, Z.; Wang, F.; Xu, R.; Tao, J.; Zhang, S.; Qin, Q.; Luther-Davies, B.; Jagadish, C.; Yu, Z.; Lu, Y. Atomically Thin Optical Lenses and Gratings. *Light: Science & Applications* **2016**, 5 (3), e16046–e16046. <https://doi.org/10.1038/lsa.2016.46>.
- (36) Ma, L.; Chen, R.; Dong, S.; Yu, T. In Situ Strain Electrical Atomic Force Microscopy Study on Two-dimensional Ternary Transition Metal Dichalcogenides. *InfoMat* **2022**. <https://doi.org/10.1002/inf2.12310>.
- (37) Munkhbat, B.; Yankovich, A. B.; Baranov, D. G.; Verre, R.; Olsson, E.; Shegai, T. O. Transition Metal Dichalcogenide Metamaterials with Atomic Precision. *Nat Commun* **2020**, 11 (1), 4604. <https://doi.org/10.1038/s41467-020-18428-2>.
- (38) Danielsen, D. R.; Lyksborg-Andersen, A.; Nielsen, K. E. S.; Jessen, B. S.; Booth, T. J.; Doan, M.-H.; Zhou, Y.; Bøggild, P.; Gammelgaard, L. Super-Resolution Nanolithography of Two-Dimensional Materials by Anisotropic Etching. *ACS Appl. Mater. Interfaces* **2021**, 13 (35), 41886–41894. <https://doi.org/10.1021/acsaami.1c09923>.

- (39) Guo, Y.; Shen, P.-C.; Su, C.; Lu, A.-Y.; Hempel, M.; Han, Y.; Ji, Q.; Lin, Y.; Shi, E.; McVay, E.; Dou, L.; Muller, D. A.; Palacios, T.; Li, J.; Ling, X.; Kong, J. Additive Manufacturing of Patterned 2D Semiconductor through Recyclable Masked Growth. *Proc. Natl. Acad. Sci. U.S.A.* **2019**, *116* (9), 3437–3442. <https://doi.org/10.1073/pnas.1816197116>.
- (40) Liu, Y.; Gu, F. A Wafer-Scale Synthesis of Monolayer MoS₂ and Their Field-Effect Transistors toward Practical Applications. *Nanoscale Adv.* **2021**, *3* (8), 2117–2138. <https://doi.org/10.1039/D0NA01043J>.
- (41) Zhang, Y.; Yao, Y.; Sendeku, M. G.; Yin, L.; Zhan, X.; Wang, F.; Wang, Z.; He, J. Recent Progress in CVD Growth of 2D Transition Metal Dichalcogenides and Related Heterostructures. *Advanced Materials* **2019**, *31* (41), 1901694. <https://doi.org/10.1002/adma.201901694>.
- (42) Martella, C.; Melloni, P.; Cinquanta, E.; Cianci, E.; Alia, M.; Longo, M.; Lamperti, A.; Vangelista, S.; Fanciulli, M.; Molle, A. Engineering the Growth of MoS₂ via Atomic Layer Deposition of Molybdenum Oxide Film Precursor. *Advanced Electronic Materials* **2016**, *2* (10), 1600330. <https://doi.org/10.1002/aelm.201600330>.
- (43) Tang, J.; Wei, Z.; Wang, Q.; Wang, Y.; Han, B.; Li, X.; Huang, B.; Liao, M.; Liu, J.; Li, N.; Zhao, Y.; Shen, C.; Guo, Y.; Bai, X.; Gao, P.; Yang, W.; Chen, L.; Wu, K.; Yang, R.; Shi, D.; Zhang, G. In Situ Oxygen Doping of Monolayer MoS₂ for Novel Electronics. *Small* **2020**, *16* (42), 2004276. <https://doi.org/10.1002/smll.202004276>.
- (44) Cohen, A.; Patsha, A.; Mohapatra, P. K.; Kazes, M.; Ranganathan, K.; Houben, L.; Oron, D.; Ismach, A. Growth-Etch Metal–Organic Chemical Vapor Deposition Approach of WS₂ Atomic Layers. *ACS Nano* **2021**, *15* (1), 526–538. <https://doi.org/10.1021/acsnano.0c05394>.
- (45) Giannazzo, F.; Bosi, M.; Fabbri, F.; Schilirò, E.; Greco, G.; Roccaforte, F. Direct Probing of Grain Boundary Resistance in Chemical Vapor Deposition-Grown Monolayer MoS₂ by Conductive Atomic Force Microscopy. *Phys. Status Solidi RRL* **2020**, *14* (2), 1900393. <https://doi.org/10.1002/pssr.201900393>.
- (46) Chiappe, D.; Asselberghs, I.; Sutar, S.; Iacovo, S.; Afanas'ev, V.; Stesmans, A.; Balaji, Y.; Peters, L.; Heyne, M.; Mannarino, M.; Vandervorst, W.; Sayan, S.; Huyghebaert, C.; Caymax, M.; Heyns, M.; De Gendt, S.; Radu, I.; Thean, A. Controlled Sulfurization Process for the Synthesis of Large Area MoS₂ Films and MoS₂/WS₂ Heterostructures. *Adv. Mater. Interfaces* **2016**, *3* (4), 1500635. <https://doi.org/10.1002/admi.201500635>.
- (47) Thangaraja, A.; Shinde, S. M.; Kalita, G.; Tanemura, M. An Effective Approach to Synthesize Monolayer Tungsten Disulphide Crystals Using Tungsten Halide Precursor. *Applied Physics Letters* **2016**, *108* (5), 053104. <https://doi.org/10.1063/1.4941393>.
- (48) Sun, H.; Dong, J.; Liu, F.; Ding, F. Etching of Two-Dimensional Materials. *Materials Today* **2021**, *42*, 192–213. <https://doi.org/10.1016/j.mattod.2020.09.031>.
- (49) He, T.; Wang, Z.; Zhong, F.; Fang, H.; Wang, P.; Hu, W. Etching Techniques in 2D Materials. *Adv. Mater. Technol.* **2019**, *4* (8), 1900064. <https://doi.org/10.1002/admt.201900064>.
- (50) Garcia, R.; Knoll, A. W.; Riedo, E. Advanced Scanning Probe Lithography. *Nature Nanotech* **2014**, *9* (8), 577–587. <https://doi.org/10.1038/nnano.2014.157>.
- (51) Albisetti, E.; Calò, A.; Zanut, A.; Zheng, X.; de Peppo, G. M.; Riedo, E. Thermal Scanning Probe Lithography. *Nat Rev Methods Primers* **2022**, *2* (1), 32. <https://doi.org/10.1038/s43586-022-00110-0>.
- (52) Liu, X.; Howell, S. T.; Conde-Rubio, A.; Boero, G.; Brugger, J. Thermomechanical Nanocutting of 2D Materials. *Adv. Mater.* **2020**, *32* (31), 2001232. <https://doi.org/10.1002/adma.202001232>.

- (53) Liu, X.; Sachan, A. K.; Howell, S. T.; Conde-Rubio, A.; Knoll, A. W.; Boero, G.; Zenobi, R.; Brugger, J. Thermomechanical Nanostraining of Two-Dimensional Materials. *Nano Lett.* **2020**, *20* (11), 8250–8257. <https://doi.org/10.1021/acs.nanolett.0c03358>.
- (54) Martella, C.; Mennucci, C.; Cinquanta, E.; Lamperti, A.; Cappelluti, E.; Buatier de Mongeot, F.; Molle, A. Anisotropic MoS₂ Nanosheets Grown on Self-Organized Nanopatterned Substrates. *Advanced Materials* **2017**, *29* (19), 1605785. <https://doi.org/10.1002/adma.201605785>.
- (55) Camellini, A.; Mennucci, C.; Cinquanta, E.; Martella, C.; Mazzanti, A.; Lamperti, A.; Molle, A.; de Mongeot, F. B.; Della Valle, G.; Zavelani-Rossi, M. Ultrafast Anisotropic Exciton Dynamics in Nanopatterned MoS₂ Sheets. *ACS Photonics* **2018**, *5* (8), 3363–3371. <https://doi.org/10.1021/acsphotonics.8b00621>.
- (56) Jeon, M. H.; Ahn, C.; Kim, H.; Kim, K. N.; LiN, T. Z.; Qin, H.; Kim, Y.; Lee, S.; Kim, T.; Yeom, G. Y. Controlled MoS₂ Layer Etching Using CF₄ Plasma. *Nanotechnology* **2015**, *26* (35), 355706. <https://doi.org/10.1088/0957-4484/26/35/355706>.
- (57) Choi, S.; Shaolin, Z.; Yang, W. Layer-Number-Dependent Work Function of MoS₂ Nanoflakes. *Journal of the Korean Physical Society* **2014**, *64* (10), 1550–1555. <https://doi.org/10.3938/jkps.64.1550>.
- (58) Kim, J. H.; Lee, J.; Kim, J. H.; Hwang, C. C.; Lee, C.; Park, J. Y. Work Function Variation of MoS₂ Atomic Layers Grown with Chemical Vapor Deposition: The Effects of Thickness and the Adsorption of Water/Oxygen Molecules. *Appl. Phys. Lett.* **2015**, *106* (25), 251606. <https://doi.org/10.1063/1.4923202>.
- (59) Pacheco, L.; Martinez, N. F. Enhanced Current Dynamic Range Using ResiScopeTM and Soft-ResiScopeTM AFM Modes. In *Conductive Atomic Force Microscopy*; John Wiley & Sons, Ltd, 2017; pp 263–276. <https://doi.org/10.1002/9783527699773.ch12>.
- (60) Greene, J. E. Quantitative Electrical Measurements with Atomic Force Microscopy. *Micros. Today* **2015**, *23* (6), 32–37. <https://doi.org/10.1017/S1551929515000991>.
- (61) Panasci, S. E.; Koos, A.; Schilirò, E.; Di Franco, S.; Greco, G.; Fiorenza, P.; Roccaforte, F.; Agnello, S.; Cannas, M.; Gelardi, F. M.; Sulyok, A.; Nemeth, M.; Pécz, B.; Giannazzo, F. Multiscale Investigation of the Structural, Electrical and Photoluminescence Properties of MoS₂ Obtained by MoO₃ Sulfurization. *Nanomaterials* **2022**, *12* (2), 182. <https://doi.org/10.3390/nano12020182>.
- (62) Hamada, T.; Tomiya, S.; Tatsumi, T.; Hamada, M.; Horiguchi, T.; Kakushima, K.; Tsutsui, K.; Wakabayashi, H. Sheet Resistance Reduction of MoS₂ Film Using Sputtering and Chlorine Plasma Treatment Followed by Sulfur Vapor Annealing. *IEEE J. Electron Devices Soc.* **2021**, *9*, 278–285. <https://doi.org/10.1109/JEDS.2021.3050801>.